Producing Bowtie Limited Diffraction Beams with Synthetic Array Experiment

Jian-yu Lu, *Member, IEEE*

Abstract— **Limited diffraction beams have a large depth of field and could have applications in medical ultrasound and other wave related areas such as electromagnetics and optics. However, these beams have higher sidelobes than conventional focused beams at their focuses. Recently, a new type of beam, called bowtie limited diffraction beams, was developed. These beams can achieve both low sidelobes and a large depth of field in medical imaging. In this paper, the production of bowtie beams in water with a synthetic array experiment is reported. A broad-band PZT ceramic/polymer composite transducer of about 1 mm diameter and 2.5 MHz central frequency was scanned in a raster format and placed at the centers of elements of an equivalent two-dimensional array of 50 mm diameter aperture. A polyvinylidene fluoride (PVDF) needle hydrophone of 0.5 mm diameter was used to receive the waves produced by the transducer. Proper weighting functions were applied to the received signals to produce various beams. Results show that the bowtie beams produced with the synthetic array experiment are in good agreement with those derived from theory and obtained by computer simulations. The depth of field of these beams is about 216 mm and sidelobes of a tenth derivative bowtie X wave in pulse–echo imaging are about 30 dB lower than those of rotary symmetric limited diffraction beams such as the zeroth-order X wave discovered previously.**

I. Introduction

THE FIRST localized waves that are exact solutions to the isotropic–homogeneous scalar wave equation were discovered in electromagnetics by Brittingham in 1983 [1]. These waves were also termed "focus wave modes" and can propagate to a large distance with only local deformation. Localized waves were further studied by Ziolkowski [2] and many other investigators [3]–[10]. Independent of Brittingham and Ziolkowski's work, in 1987, Durnin first studied experimentally limited diffraction beams that have a pencil-like beam shape [11]. These beams are different from localized waves because in theory they can propagate to an infinite distance without changing beam shapes (having an infinite depth of field) if they are produced with an infinite aperture. Even if produced with a finite aperture, they have a large depth of field. Durnin has termed these new beams "nondiffracting beams" [11] or "diffraction-free beams" [12]. Because Durnin's terminologies are controversial in the scientific community, the new term "limited diffraction beams" [13] has been used on the basis that all practical beams will diffract eventually. Durnin's beams are also called Bessel beams because their lateral profiles are a Bessel function. Durnin's beams have been further studied in both optics [14]–[17] and acoustics [18], [19]. Recently, a new family of limited diffraction beam was discovered [20], [21]. These beams are called X waves because they have an "X-like" shape in a plane along their axes. X waves are different from Bessel beams because they are nondispersive in an isotropic–homogeneous medium. This property may be useful for improving the quality of images obtained by X wave pulse–echo systems with deconvolution because the point spread function of these systems would be depth independent. Because limited diffraction beams have a large depth of field, they could have applications in medical imaging [22]–[30], tissue characterization [31], Doppler flow velocity measurement [32], volumetric imaging [33], nondestructive evaluation (NDE) of materials [34], and other areas such as electromagnetics [7] and optics [17].

Although limited diffraction beams have a large depth of field, they have higher sidelobes than conventional focused beams at their focuses. High sidelobes may lower contrast of medical imaging and make detection of low-contrast objects such as small cysts difficult. A summation–subtraction method has been proposed to reduce sidelobes of limited diffraction beams [35]. This method is similar to those developed by Wild [36], Burckhardt *et al*. [37], and Patterson *et al*. [38], for the electromagnetic ring antenna, ultrasound ring transducer, and Axicon transducer, respectively. However, the summation–subtraction method has several drawbacks. First, it lowers image frame rate because multiple transmissions are needed to obtain an A-line. Second, it is sensitive to object motion because the summation and subtraction are done for RF echo signals. Third, the final images have a small dynamic range in the presence of noise because large pulse–echo signals are subtracted and only the small differences are of interest. Other methods for sidelobe reduction such as using localized waves [39] were also proposed. Their limitations were reviewed in [13].

Recently, a new type of limited diffraction beam was developed [26]. These beams are called bowtie limited diffraction beams because they have a bowtie shape in a plane perpendicular to the beam axis. Sidelobes of these beams are angle (around the axis) dependent. With bowtie limited diffraction beams, pulse–echo systems that have both low sidelobes and a large depth of field could be constructed. In these systems, a bowtie beam is used in transmission and its 90° rotated beam pattern (around the beam axis) is in reception [26]. Unlike the summation–subtraction method, this

Manuscript received July 28, 1995; revised May 1, 1996. This work was supported in part by Grants CA 54212 and CA 43920 from the National Institutes of Health.

The author is with the Biodynamics Research Unit, Department of Physiology and Biophysics, Mayo Clinic and Foundation, Rochester, MN 55905 USA (e-mail: jian@mayo.edu).

Publisher Item Identifier S 0885-3010(96)06329-0.

method can reduce sidelobes dramatically without lowering image frame rate.

Because bowtie limited diffraction beams are angle dependent, a two-dimensional (2-D) array is required to produce them experimentally. Since dense 2-D arrays are difficult to construct and are not currently available, in this paper a synthetic array experiment was designed to produce these beams in water and to verify the theory and computer simulations [26]. In the experiment, a small single-element 2.5-MHz central frequency and wide-band PZT ceramic/polymer composite transducer was used to produce ultrasonic waves, and a small (0.5 mm diameter) and broad-band polyvinylidene fluoride (PVDF) needle hydrophone was used to measured the waves. When the amplitude of the waves is small, which was the case in the experiment, the experiment system is approximately linear. This means that when a single-element transducer is placed at the centers of elements of an imagined 2-D array and transmits waves sequentially, the summation of signals received by a hydrophone will be equal to that produced by the 2-D array with its elements transmitting simultaneously (ignore the crosstalk of the array and assume that environment conditions remain the same during the experiment). Because the system is approximately linear, the aperture weightings applied to the 2-D array to produce bowtie beams can also be applied to the received signals produced sequentially by the single-element transducer. This is an advantage because the same set of data obtained from the experiment can be used to produce other limited diffraction beams [33] by adding different weighting functions.

In the following, the theory of bowtie limited diffraction beams will be reviewed briefly. Then, the synthetic array experiment will be described in detail and results will be compared with those obtained from the theory and computer simulations. Finally, a brief discussion and conclusion will be given.

II. Theory

Bowtie limited diffraction beams are exact solutions to the isotropic–homogeneous scalar wave equation [26]. They are obtained from derivatives in one transverse direction, say, y, of the rotary symmetric (around beam axis) limited diffraction beams such as the zeroth-order X wave [20], [21]

$$\Phi_{XBB_0}(r, z - c_1 t) = \frac{a_0}{\sqrt{(r\sin\zeta)^2 + [a_0 - i\cos\zeta(z - c_1 t)]^2}} \tag{1}$$

and Bessel beam [11], [12]

$$\Phi_{J_0}(r, z - c_1 t) = A J_0(\alpha r) e^{i(\beta z - \omega t)} \tag{2}$$

where $r = \sqrt{x^2 + y^2}$, z is axial distance, t is time, $c_1 = c/\cos\zeta$ and $c_1 = c/\beta$ are for X waves and Bessel beams, respectively, c is the speed of sound or light of the medium, ζ is the Axicon angle [20], a_0 is a constant that determines the decay speed of the high-frequency components of X waves, A is a complex constant, J_0 is the zeroth-order Bessel function of the first kind, α is a parameter that determines the main beamwidth of Bessel beams, and $\beta = \sqrt{k^2 - \alpha^2} > 0$ is a propagation constant, where $k = \omega/c$ is the wavenumber and ω is the angular frequency.

The mth-derivative bowtie X wave and Bessel beam are given by [26]

$$\Phi_{X_{B_m}}(r, \phi, z - c_1 t) = \frac{\partial^m}{\partial y^m} \Phi_{XBB_0}(r, z - c_1 t) \tag{3}$$

and

$$\Phi_{J_{B_m}}(r, \phi, z - c_1 t) = \frac{\partial^m}{\partial y^m} \Phi_{J_0}(r, z - c_1 t) \tag{4}$$

respectively, where the subscript B_m means mth-derivative bowtie waves, m is a nonnegative even integer and is the order of the derivatives, and ϕ is the polar angle in the x–y plane. Because Bessel beams are a special case of X waves [20], in the following, only bowtie X waves are studied. Furthermore, $m = 4$ and 10 are chosen to show the trend of bowtie X waves with the order of derivatives.

From (3) and (4), one sees that the bowtie beams are angle (ϕ) dependent. Beam amplitude is high for $\pi/4 < \phi < 3\pi/4$ and $5\pi/4 < \phi < 7\pi/4$, and is low for $-\pi/4 < \phi < \pi/4$ and $3\pi/4 < \phi < 5\pi/4$. As the order of derivative increases, higher amplitude of the beam will be concentrated around the y axis and the lower amplitude will be around the x axis. This makes bowtie beams attractive for sidelobe reduction in pulse–echo imaging because one can transmit a bowtie beam and then rotate electronically the beam pattern by 90° during receive. Sidelobes of the beams will be suppressed during the pulse–echo process while the center peak of the beam remains, i.e., pencil beams are formed. For more details of the beam patterns one can refer to [26] where transverse views of the bowtie X waves in (3) for $m = 4$ and 10 are shown [images of peaks of the waveforms, $\max\{\Phi_{X_{B_m}}(-c_1 t)\}$, at $z = 0$ for all transverse positions (r, ϕ)].

In practice, a bowtie beam can only be approximately produced with a finite aperture. In this case, the depth of field of the beam is no longer infinite, but is given by [26]

$$XZ_{\max} = \frac{D}{2}\cot\zeta \tag{5}$$

where D is the diameter of the aperture and ζ is the Axicon angle [20]. Because theoretically the beamwidth of a limited diffraction beam will not change with axial distance, z, this definition of the depth of field is different from that of a conventional focused beam. For limited diffraction beams, the depth of field is defined as the distance from the surface of a transducer at which the peak amplitude of the beams drops by 6 dB as compared to that at the transducer surface. Within the depth of field, limited diffraction beams are close to the theoretical beams and their lateral beamwidth and sidelobes do not change significantly with distance. However, at or beyond the depth of field, beamwidth and sidelobes may have a dramatic increase.

III. Synthetic Array Experiment

In this section, the synthetic array experiment for producing bowtie limited diffraction beams is described.

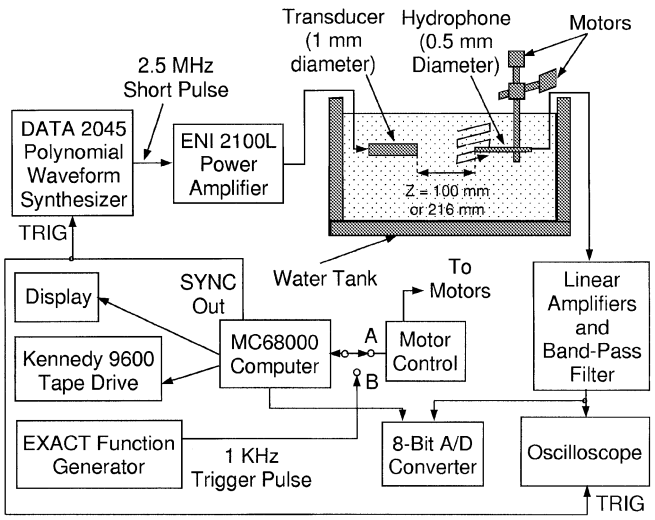

Fig. 1. Block diagram of a synthetic array experiment for producing limited diffraction beams in water.

A block diagram of the synthetic array experiment is shown in Fig. 1. A polynomial waveform synthesizer (ANALOGIC DATA 2045) was used to produce a short pulse of about one-and-a-half cycle and of a center frequency of about 2.5 MHz. The pulse was amplified by a power amplifier (ENI 2100L) to produce a peak amplitude of about 100 V and to drive a 2.5-MHz broad-band single-element transducer that was immersed in a water tank. The single-element transducer (actually, the central element of an annular array [23] made by Echo Ultrasound[1]) was made from PZT ceramics/polymer composite material and its diameter was about 4 mm. To reduce the size of the transducer, a foam tape (3M Microfoam[2]) punched with a ping hole that had about 1 mm diameter and 1 mm thickness was attached to the front surface of the transducer and aligned with the center of the element. The transfer function of the transducer was similar to that of a one-way Blackman window function [40] which had a -6 dB relative bandwidth (bandwidth divided by the central frequency) of about 81%. This spectrum was similar to that used in the theory and computer simulations published previously (see [26, Figs. 4–7]).

The acoustic waves produced by the transducer were measured with a broad-band PVDF needle hydrophone (NTR 1000[3]) of 0.5 mm diameter. The measured signals were amplified, band-pass filtered, and digitized. To automate the measurement, the hydrophone was scanned by step motors in a raster format in a plane some distance (100 or 216 mm) away from the transducer. The motors run continuously and data were collected while the motors were in motion [the scanning speed of hydrophone was about 60 mm/s and thus its motion was almost "frozen" during each data acquisition (15 μs maximum)]. To remove backlashes of the scanning system, data were acquired only in one scan direction of the hydrophone (e.g., from front to back, see Fig. 1).

[1] A Division of ATL, Reedsville, PA.

[2] 3M Commercial Office Supply Division, St. Paul, MN.

[3] NTR System, Inc., Seattle, WA.

At each position of the hydrophone (controlled by counting the number of pulses sent to the step motors), a motor controller sent out a trigger signal to the computer (MC68000) that produced a new trigger synchronized with the clock of the delay unit of the A/D converter (the synchronization removes the jittering of the delay time). The synchronized trigger was used to produce the excitation signal of the transducer. After a preset delay time (143 μs maximum), the A/D converter (8-bit) digitized the signal from the hydrophone and stored the data in the computer memory and then in a hard disk. The data were also displayed on a monitor of the computer for viewing. The stored data were then transferred via a tape drive (Kennedy 9600) to a SUN SPARC 2 workstation for processing. Before data acquisition, the system was aligned using an oscilloscope (Tektronix 2445 150 MHz) that was synchronized with an alternative trigger source (1 KHz) produced by a function generator (EXACT Model 129) [the switch on the computer was connected to post B (Fig. 1)].

Because the motion between the hydrophone and the single-element transducer is relative, the scanning of the hydrophone is equivalent to the scan of the transducer with the hydrophone fixed. In the experiment, the hydrophone was scanned because it was lighter in weight and would cause less mechanical vibration. In the following, we assume that the transducer is scanned and the hydrophone is fixed in space.

Theoretically, bowtie limited diffraction beams must be produced with an infinite aperture. In practice, they can be produced approximately [26] over a large depth of field with a 2-D array transducer of a finite aperture and of a sufficiently large number of elements (minimum number of elements is determined by the Nyquist sampling theorem) [21], [23], [28]. Unfortunately, 2-D arrays of a large number of elements are difficult to construct and are not currently available. However, if the experiment system in Fig. 1 is linear and the experiment time is short so that the environment conditions remain about the same during the experiment, synthetic arrays can be used to replace a 2-D array to produce bowtie beams. In the above synthetic array experiment, the amplitude of waves produced by the single-element transducer was made as small as possible so that the system was approximately linear. The experiment time was relatively short (less than 20 min) because a continuous scan (would need about four days for a stepped scan where motors are turned off during data acquisitions) was used. In addition, to minimize the changes of environment parameters such as the temperature, 200 L of water were used in an air-conditioned room. Phase shift caused by any change of temperature during the experiment is negligible. A synthetic array was formed by placing the single-element transducer sequentially on where the centers of elements of a 2-D array would exist. At each position, the transducer was weighted accordingly and wave was transmitted. The waves were received by the hydrophone and summed coherently later in a computer to reconstruct the field response of the synthetic array at the hydrophone position. Because the system is assumed linear, the field response is equal to that produced by the 2-D array with its elements transmitting simultaneously. Alternatively, aperture weightings of the synthetic arrays can be applied to the

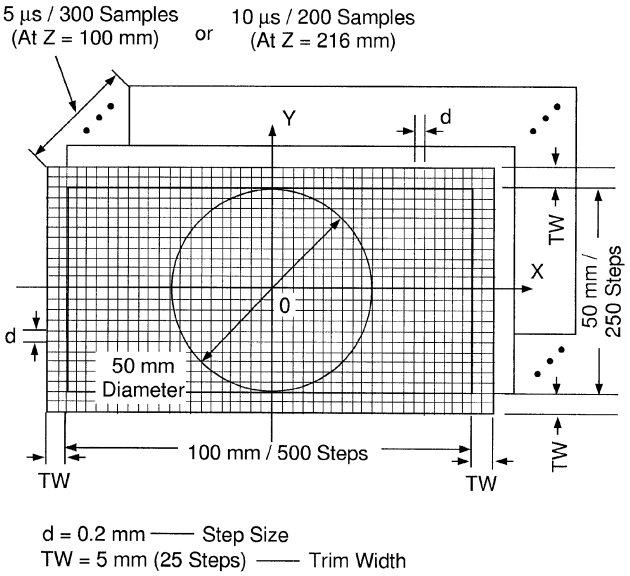

Fig. 2. Geometry of data acquisition in synthetic array experiment.

received signals so that they can be changed later in a computer to produce various beams with the same set of data. To produce bowtie X waves, the weighting function is given by (3) evaluated at $z = 0$. Other limited diffraction beams can be obtained by applying different weighting functions [33].

To produce field responses of bowtie beams on a lateral line perpendicular to the beam axis, an area that was larger than the aperture of the beams was scanned. In the synthetic array experiment, the area was 110 mm $\times$ 60 mm (Fig. 2) with a step size of 0.2 mm (distance between two neighboring transmitting positions) in both the x and y directions. Waves transmitted within this area were measured with the hydrophone located at $z = 100$ and 216 mm, and digitized at a rate of 20 megasamples/second for 15 μs (300 samples) and 10 μs (200 samples), respectively. To produce bowtie beams, weighting functions were applied to a 50 mm diameter aperture (Fig. 2) and the hydrophone was centered at the z axis. Waves produced within this aperture were coherently summed and lateral line plots (from -25 to 25 mm) of the beams were obtained by shifting the weighting aperture horizontally along the x axis in 0.2-mm steps. To obtain a line plot along a different angle, $\phi = \tan^{-1} y/x$, the weighting functions were rotated around the beam axis by that angle. Because the alignment of the hydrophone may not be perfectly on the z axis, a trim area that had a 5 mm width was reserved on each side of the scanning area (Fig. 2). This trim allows a software reposition of the center of the x–y coordinates or the alignment of the center of the 50 mm diameter aperture.

IV. Results

Because bowtie limited diffraction beams have a strong angular dependency (strong function of ϕ), they can be applied to pulse–echo systems for low sidelobe and large depth of field imaging [26]. In these systems, a bowtie beam is used in transmission and its 90° rotated response is used in reception (the aperture weighting function in reception is rotated around the beam axis, z, by 90°). Because the pulse–echo response of a system is a convolution of the transmission and reception beam patterns with respect to time, sidelobes of such systems are greatly reduced.

Line plots of the pulse–echo responses of the fourth and tenth derivative bowtie X waves obtained from the synthetic array experiment are shown in Figs. 3 and 4, respectively. For comparison, the line plots from the theory and computer simulations (the theory and simulation mean the analytic solutions to the wave equation and the results obtained with the Rayleigh–Sommerfeld diffraction formula, respectively) are also shown [26]. To compare with the rotary symmetric limited diffraction beams, the line plot of the zeroth-order X wave [20] that was obtained from the data of the same synthetic array experiment is included in the plots.

Cross-sectional images of the fourth and tenth derivative bowtie X waves obtained from the synthetic array experiment at $z = 100$ mm and at two angles, $\phi = 0°$ and 90°, in an r–z plane are shown in Fig. 5. Results from the zeroth-order X wave are also shown. The depth of field (216 mm) [26] of the bowtie beams in Figs. 3–5 is the same as that of the zeroth-order X wave because the aperture diameter and the Axicon angle of these beams are the same [26]. Simulation and theoretical results corresponding to Fig. 5 are in [26, Figs. 6 and 7, respectively]. Notice that in Figs. 3–5, the beams in the lateral distance from -25 mm to 0 are mirrored from 0 to 25 mm because the beams should be symmetric in these figures.

V. Discussion

Bowtie limited diffraction beams could be applied to pulse–echo systems for low sidelobe and large depth of field imaging [26]. In this paper, a synthetic array experiment (Figs. 1 and 2) was developed to produce these beams. The results (Figs. 3–5) compare very well with those obtained previously from the theory and computer simulations (see [26, Figs. 4–7]). Sidelobes of pulse–echo responses of bowtie limited diffraction beams, especially those of higher derivatives, are reduced dramatically from those of the rotary symmetric limited diffraction beams (Figs. 3 and 4) [20]. These results demonstrate that our experiment system is approximately linear and the bowtie beam formation is not sensitive to the inevitable imperfect conditions in the experiment. The results also show that the main beamwidth of the bowtie beams are about the same at two different distances (one is within the depth of field and the other is at the boundary of the depth of field) and is close to that predicted by theory and computer simulations. This means that the beams obtained by the experiment have about the same depth of field as those obtained by the theory and simulation (see [26, Fig. 8]).

The use of a synthetic array in the experiment has several advantages over that of a 2-D array. Synthetic arrays use only a single-element transducer and a single-channel power amplifier which simplify the experiment. In addition, it is flexible to produce either limited diffraction beams [33] or conventional focused beams with the same data from a synthetic array experiment because different aperture weighting functions can be applied after the experiment. Moreover, a synthetic array does not have any acoustical or electrical crosstalk among

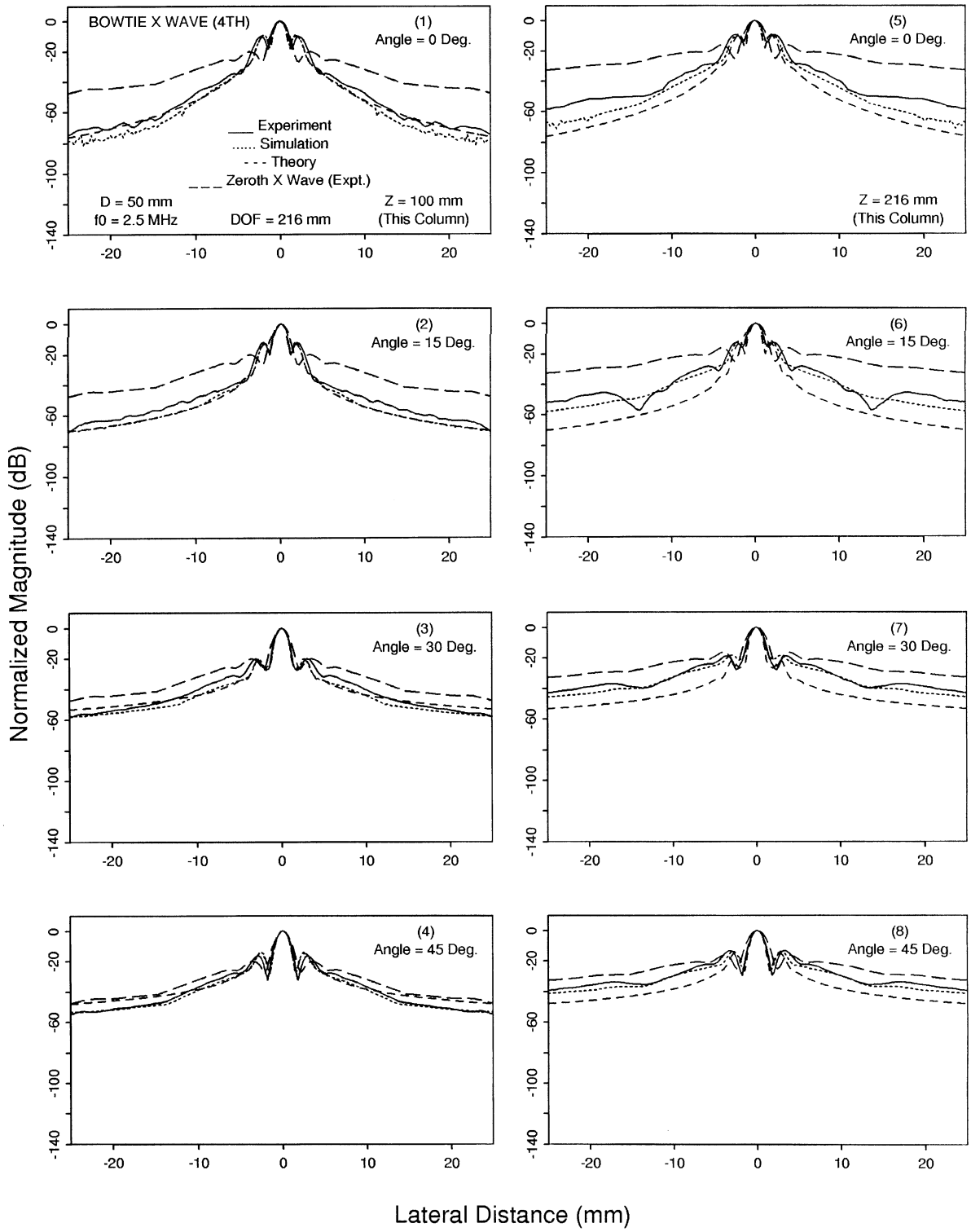

Fig. 3. Line plots of the pulse–echo (two-way) responses of the fourth derivative bowtie X wave (full lines) obtained from the synthetic array experiment at four different angles: 0° (the first row), 15° (the second row), 30° (the third row), and 45° (the bottom row), and at two axial distances: $z = 100$ mm (left column) and 216 mm (right column). In the pulse–echo responses, a fourth derivative bowtie X wave was used in transmission and its 90° rotated response (the aperture weighting function was rotated around the beam axis, z, by 90°) was used in reception. The pulse–echo beam pattern was obtained with the convolution of the signals of the transmission and reception with respect to time. The line plots are the peaks of the absolute values of the pulse–echo responses over the lateral distance; this gives the maximum sidelobes. The plots are compared with those obtained by computer simulations (dotted lines) [26], theory (dashed lines) [26], and the zeroth-order X wave [20] (long dashed lines). In both the theory and simulations, the spectrum of the pulse–echo responses was assumed to be a two-way Blackman window function and the -6 dB bandwidth was about 58% of the central frequency (2.5 MHz). The plots were obtained with the following parameters: the diameter of the aperture of the synthetic array was 50 mm; the Axicon angle, ζ, was 6.6°; and the constant, a_0, that controls the fall-off speed of the high-frequency components of X waves were 0.10 and 0.03 mm for the fourth derivative bowtie X wave and the zeroth-order X wave, respectively. The vertical axis is from 0 to -140 dB and the horizontal is from -25 to 25 mm.

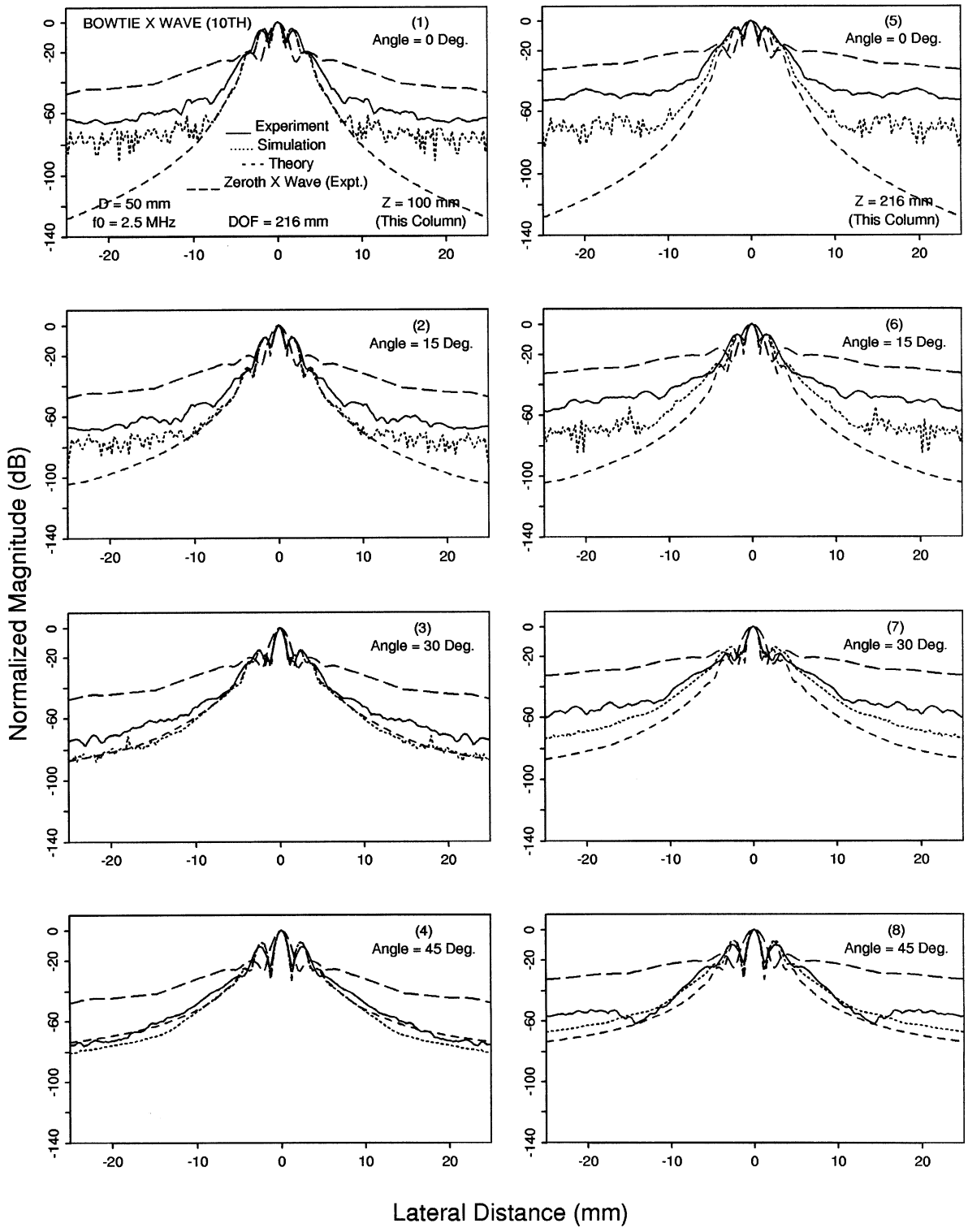

Fig. 4. The same format as Fig. 3 except for the pulse–echo responses of the tenth derivative bowtie X wave. The parameters of the beams are also the same as those of Fig. 3 except that $a_0 = 0.15$ mm for the bowtie beam in this figure. The increased sidelobes from those of the theory in the panels of the first two rows were caused by the numerical errors in the computer simulations (dotted lines) and the noise of the synthetic array experiment (full lines). The noise of the experiment is explained in Section V.

its elements and the properties of each element are exactly the same. The change of the size of the elements or the interelement distance of synthetic arrays is relatively easy. The size of the elements can even be larger than the interelement distance (the size of the element is about 1 mm and the interelement distance is 0.2 mm in the above experiment). This overlap of elements increases the total acoustic power transmitted and improve the signal-to-noise ratio (SNR) of the data at the expense of the requirement for a larger data storage and a longer data acquisition time.

Although synthetic arrays have many advantages, there are limitations. First, the experiment system must be as close to

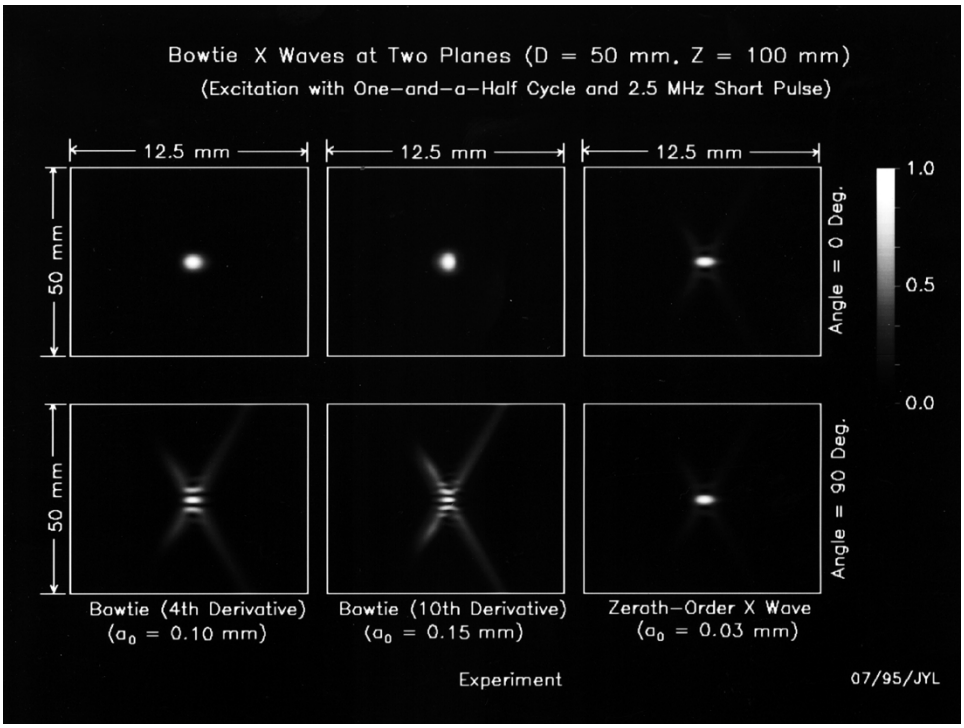

Fig. 5. One-way (transmission or reception) fourth (panels in the left column) and tenth derivative (panels in the middle column) bowtie X waves shown in the plane (r–z plane) along the wave axis and obtained with the synthetic array experiment at the axial distance, $z = 100$ mm, and at two angles: $\phi = 0^\circ$ (panels in the upper row) and 90° (panels in the bottom row). The zeroth-order X wave (panels in the right column) is added for comparison. The parameters used in this figure are the same as those in Figs. 3 and 4. The gray scale of the images in the panels is proportional to the analytic envelope of the real part of the waves; it is linear and normalized to the range from 0.0 to 1.0 in 256 levels.

linear as possible so that the arrays can be synthesized with linear superpositions without severe beam distortion. Second, the beamforming is slow. This is because the beam produced at an observation point is the summation of the waves transmitted sequentially from a single-element transducer that is scanned over the entire array aperture. The sequential beamforming requires that the conditions of the media in which beams propagate do not change during the experiment. Third, a large amount of RF data is required to construct a beam. The amount of data increases with the number of transmissions in the array aperture and the number of samples acquired during each transmission. With the example given in Section III (assuming that each sample is 1-byte or 8-bit long), the amounts of data acquired are 49.5 and 33 MB for $z = 100$ and 216 mm, respectively, including the data in the trim areas (Fig. 2). Finally, because the size of the single-element transducer is small and the acoustic wave from the transducer decays quickly with distance, the SNR of the received signals is low. In the above examples where the axial distances were 100 and 216 mm and the size of the transducer element was 1 mm, the measured signals were noisy even if they were digitized with a low resolution (8-bit) A/D converter (the major noise was from stray electromagnetic field of running step motors). This is seen from Fig. 4 where the noise actually dominates the extremely low sidelobes of the pulse–echo responses (see the panels in the first two rows) of the tenth derivative bowtie X wave. The noise at the larger distance ($z = 216$ mm or panels in the right column of Fig. 4) is even higher.

One way to reduce noise is to increase the transmission power by increasing the excitation voltage. However, this increases the intensity of the acoustic wave near the surface of the transducer and may cause distortions due to nonlinearity and cavitation. High voltage may also damage the transducer (as a compromise, a pulse of 100 V peak amplitude was used in the above experiment). The other way to reduce the noise is to increase the size of the transducer element. However, this is limited by the accuracy of the stepwise approximation of the aperture weighting function and the increased directivity of the element. Finally, the motor noise can be removed by stopping the motor completely during each data acquisition. Nevertheless, this increases the data acquisition time dramatically since the hydrophone must be settled for a few seconds to reduce its mechanical vibration before data acquisitions and thus the environment parameters such as temperature and gain of amplifiers may change during the experiment. Although the SNR is low in the single-element transmission, the coherent summation of all the transmissions to form a beam may cancel some of additive noise. This is seen from Fig. 4 where the noise level is around -60 dB which is much lower than that of the single-element transmission. The noise could be reduced further if a 2-D array is used. However, such arrays are not currently available.

VI. Conclusion

Bowtie limited diffraction beams could have both low sidelobes and a large depth of field in medical imaging even if they are produced with a finite aperture. In this paper, a synthetic array experiment was developed to produce these beams in water. The experiment results are in good agreement with those obtained previously from theory and computer

simulations [26]. In addition, data obtained in the experiment can also be used to produce other limited diffraction beams [33]. The experiment verifies the theory and simulations, and demonstrates the feasibility of producing bowtie limited diffraction beams.

ACKNOWLEDGMENT

The author appreciates the secretarial assistance of E. C. Quarve.

REFERENCES

[1] J. N. Brittingham, "Focus wave modes in homogeneous Maxwell's equations: Transverse electric mode," *J. Appl. Phys.*, vol. 54, no. 3, pp. 1179–1189, 1983.
[2] R. W. Ziolkowski, "Exact solutions of the wave equation with complex source locations," *J. Math. Phys.*, vol. 26, no. 4, pp. 861–863, Apr. 1985.
[3] R. W. Ziolkowski, D. K. Lewis, and B. D. Cook, "Evidence of localized wave transmission," *Phys. Rev. Lett.*, vol. 62, no. 2, pp. 147–150, Jan. 9, 1989.
[4] A. M. Shaarawi, I. M. Besieris, and R. W. Ziolkowski, "Localized energy pulse train launched from an open, semi-infinite, circular waveguide," *J. Appl. Phys.*, vol. 65, no. 2, pp. 805–813, 1989.
[5] I. M. Besieris, A. M. Shaarawi, and R. W. Ziolkowski, "A bidirectional traveling plane wave representation of exact solutions of the scalar wave equation," *J. Math. Phys.*, vol. 30, no. 6, pp. 1254–1269, 1989.
[6] E. Heyman, B. Z. Steinberg, and L. B. Felsen, "Spectral analysis of focus wave modes," *J. Opt. Soc. Amer. A*, vol. 4, no. 11, pp. 2081–2091, Nov. 1987.
[7] R. W. Ziolkowski, "Localized transmission of electromagnetic energy," *Phys. Rev. A.*, vol. 39, no. 4, pp. 2005–2033, Feb. 15, 1989.
[8] J. V. Candy, R. W. Ziolkowski, and D. K. Lewis, "Transient waves: Reconstruction and processing," *J. Acoust. Soc. Amer.*, vol. 88, no. 5, pp. 2248–2258, Nov. 1990.
[9] ———, "Transient wave estimation: A multichannel deconvolution application," *J. Acoust. Soc. Amer.*, vol. 88, no. 5, pp. 2235–2247, Nov. 1990.
[10] R. W. Ziolkowski and D. K. Lewis, "Verification of the localized wave transmission effect," *J. Appl. Phys.*, vol. 68, no. 12, pp. 6083–6086, Dec. 15, 1990.
[11] J. Durnin, "Exact solutions for nondiffracting beams. I. The scalar theory," *J. Opt. Soc. Amer. A*, vol. 4, no. 4, pp. 651–654, 1987.
[12] J. Durnin, J. J. Miceli, Jr., and J. H. Eberly, "Diffraction-free beams," *Phys. Rev. Lett.*, vol. 58, no. 15, pp. 1499–1501, Apr. 13, 1987.
[13] J. Lu, H. Zou, and J. F. Greenleaf, "Biomedical ultrasound beam forming," *Ultrason. Med. Biol.*, vol. 20, no. 5, pp. 403–428, July 1994.
[14] G. Indebetow, "Nondiffracting optical fields: Some remarks on their analysis and synthesis," *J. Opt. Soc. Amer. A*, vol. 6, no. 1, pp. 150–152, Jan. 1989.
[15] K. Uehara and H. Kikuchi, "Generation of near diffraction-free laser beams," *Appl. Phys. B*, vol. 48, pp. 125–129, 1989.
[16] L. Vicari, "Truncation of nondiffracting beams," *Optics Commun.*, vol. 70, no. 4, pp. 263–266, Mar. 15, 1989.
[17] J. Ojeda-Castaneda and A. Noyola-lglesias, "Nondiffracting wavefields in grin and free-space," *Microwave Opt. Technol. Lett.*, vol. 3, no. 12, pp. 430–433, Dec. 1990.
[18] D. K. Hsu, F. J. Margetan, and D. O. Thompson, "Bessel beam ultrasonic transducer: Fabrication method and experimental results," *Appl. Phys. Lett.*, vol. 55, no. 20, pp. 2066–2068, Nov. 13, 1989.
[19] J. A. Campbell and S. Soloway, "Generation of a nondiffracting beam with frequency independent beam width," *J. Acoust. Soc. Amer.*, vol. 88, no. 5, pp. 2467–2477, Nov. 1990.
[20] J. Lu and J. F. Greenleaf, "Nondiffracting X waves—Exact solutions to free-space scalar wave equation and their finite aperture realizations," *IEEE Trans. Ultrason., Ferroelect., Freq. Contr.,* vol. 39, pp. 19–31, Jan. 1992.
[21] ———, "Experimental verification of nondiffracting X waves," *IEEE Trans. Ultrason., Ferroelect., Freq. Contr.,* vol. 39, pp. 441–446, May 1992.
[22] J. Lu, T. K. Song, R. R. Kinnick, and J. F. Greenleaf, "*In vitro* and *in vivo* real-time imaging with ultrasonic limited diffraction beams," *IEEE Trans. Med. Imag.,* vol. 12, pp. 819–829, Dec. 1993.
[23] J. Lu and J. F. Greenleaf, "Ultrasonic nondiffracting transducer for medical imaging," *IEEE Trans. Ultrason., Ferroelect., Freq. Contr.,* vol. 37, pp. 438–447, Sept. 1990.
[24] ———, "Pulse-echo imaging using a nondiffracting beam transducer," *Ultrason. Med. Biol.,* vol. 17, no. 3, pp. 265–281, May 1991.
[25] ———, "Diffraction-limited beams and their applications for ultrasonic imaging and tissue characterization," in *New Developments in Ultrasonic Transducers and Transducer Systems,* F. L. Lizzi, Ed., in *Proc. SPIE*, vol. 1733, pp. 92–119, 1992.
[26] J. Lu, "Bowtie limited diffraction beams for low-sidelobe and large depth of field imaging," *IEEE Trans. Ultrason., Ferroelect., Freq. Contr.,* vol. 42, pp. 1050–1063, Nov. 1995.
[27] J. Lu, H. Zou, and J. F. Greenleaf, "A new approach to obtain limited diffraction beams," *IEEE Trans. Ultrason., Ferroelect., Freq. Contr.*, vol. 42, pp. 850–853, Sept. 1995.
[28] J. Lu and J. F. Greenleaf, "A study of two-dimensional array transducers for limited diffraction beams," *IEEE Trans. Ultrason., Ferroelect., Freq. Contr.*, vol. 41, pp. 724–739, Sept. 1994.
[29] T. K. Song, J. Lu, and J. F. Greenleaf, "Modified X waves with improved field properties," *Ultrason. Imag.,* vol. 15, no. 1, pp. 36–47, Jan. 1993.
[30] M. Fatemi and M. A. Arad, "A novel imaging system based on non-diffracting X waves," in *IEEE 1992 Ultrason. Symp. Proc.*, 92CH3118-7, vol. 1, pp. 609–612.
[31] J. Lu and J. F. Greenleaf, "Evaluation of a nondiffracting transducer for tissue characterization," in *IEEE 1990 Ultrason. Symp. Proc.,* 90CH2938-9, vol. 2, pp. 795–798.
[32] J. Lu, X.-L. Xu, H. Zou, and J. F. Greenleaf, "Application of Bessel beam for Doppler velocity estimation," *IEEE Trans. Ultrason., Ferroelect., Freq. Contr.*, vol. 42, pp. 649–662, July 1995.
[33] J. Lu, "Limited diffraction array beams," *Int. J. Imag. Syst. Technol.*, to be published.
[34] J. Lu and J. F. Greenleaf, "Producing deep depth of field and depth-independent resolution in NDE with limited diffraction beams," *Ultrason. Imag.,* vol. 15, no. 2, pp. 134–149, Apr. 1993.
[35] ———, "Sidelobe reduction for limited diffraction pulse-echo systems," *IEEE Trans. Ultrason., Ferroelect., Freq. Contr.,* vol. 40, pp. 735–746, Nov. 1993.
[36] J. P. Wild, "A new method of image formation with annular apertures and application in radio astronomy," in *Proc. Roy. Soc., A,* vol. 286, pp. 499–509, 1965.
[37] C. B. Burckhardt, P. A. Grandchamp, and H. Hoffmann, "Methods for increasing the lateral resolution of B-scan," in *Acoustic Holography,* vol. 5, P. S. Green, Ed. New York: Plenum, 1973, pp. 391–413.
[38] M. S. Patterson, F. S. Foster, and D. Lee, "Sidelobe and speckle reduction for an eight sector conical scanner," in *IEEE 1981 Ultrason. Symp. Proc.*, 81CH1689-9, vol. 2, pp. 632–637.
[39] J. Lu and J. F. Greenleaf, "Comparison of sidelobes of limited diffraction beams and localized waves," *Acoust. Imag.,* J. P. Jones, Ed., vol. 21, pp. 145–152, 1995.
[40] A. V. Oppenheim and R. W. Schafer, *Digital Signal Processing*. Englewood Cliffs, NJ: Prentice-Hall, 1975, ch. 5.

Jian-yu Lu (M'88) was born in Fuzhou, Fujian Province, People's Republic of China. He received the B.S. degree in electrical engineering in February 1982 from Fudan University, Shanghai, China, the M.S. degree in 1985 from Tongji University, Shanghai, China, and the Ph.D. degree in 1988 from Southeast University, Nanjing, China.

He was a Faculty Member of the Department of Biomedical Engineering, Southeast University, Nanjing, China and worked with Prof. Y. Wei. From December 1988 to February 1990, he was a postdoctoral Research Fellow at the Biodynamics Research Unit, Mayo Clinic, Rochester, MN, and from March 1990 to December 1991, he was a Research Associate. He has been an Assistant Professor of Biophysics at the Mayo Medical School since 1991, and an Associate Consultant at the Biodynamics Research Unit, Department of Physiology and Biophysics, Mayo Clinic, since 1992. His research interests are in acoustic imaging and tissue characterization, medical ultrasonic transducers, and ultrasonic beam forming and propagation.

Dr. Lu is a recipient of the Outstanding Paper Award for two papers published in the 1992 IEEE TRANSACTIONS ON ULTRASONICS, FERROELECTRICS, AND FREQUENCY CONTROL. He is a member of the IEEE UFFC Society, the American Institute of Ultrasound in Medicine, and Sigma Xi.